RAA 2014 Vol. **14** No. **5**, 581–588 doi: 10.1088/1674–4527/14/5/007
http://www.raa-journal.org *http://www.iop.org/journals/raa*

Research in Astronomy and Astrophysics

Dependence of the length of solar filament threads on the magnetic configuration *

Yu-Hao Zhou[1,2], Peng-Fei Chen[1,2], Qing-Min Zhang[3] and Cheng Fang[1,2]

[1] School of Astronomy and Space Science, Nanjing University, Nanjing 210093, China; *yuhaozhou1991@gmail.com; chenpf@nju.edu.cn*
[2] Key Laboratory of Modern Astronomy & Astrophysics, Nanjing University, Nanjing 210093, China
[3] Purple Mountain Observatory, Chinese Academy of Sciences, Nanjing 210008, China

Received 2013 December 2; accepted 2013 December 27

Abstract High-resolution Hα observations indicate that filaments consist of an assembly of thin threads. In quiescent filaments, the threads are generally short, whereas in active region filaments, the threads are generally long. In order to explain these observational features, we performed one-dimensional radiative hydrodynamic simulations of filament formation along a dipped magnetic flux tube in the framework of the chromospheric evaporation-coronal condensation model. The geometry of a dipped magnetic flux tube is characterized by three parameters, i.e., the depth (D), the half-width (w) and the altitude (h) of the magnetic dip. A survey of the parameters in numerical simulations shows that when allowing the filament thread to grow in 5 days, the maximum length ($L_{\rm th}$) of the filament thread increases linearly with w, and decreases linearly with D and h. The dependence is fitted into a linear function $L_{\rm th} = 0.84w - 0.88D - 2.78h + 17.31$ (Mm). Such a relation can qualitatively explain why quiescent filaments have shorter threads and active region filaments have longer threads.

Key words: Sun: filaments, prominences — methods: numerical — hydrodynamics

1 INTRODUCTION

Filaments, which are also called solar prominences when they appear above the solar limb, are cold, dense concentrations of plasma in the corona (Tandberg-Hanssen 1995). They often appear as a narrow spine above the magnetic polarity inversion line (Zirker 1989; Martin 1998; Berger et al. 2008; Ning et al. 2009). Because of the large density and hence the large gravity, filament threads are often considered to be supported by the magnetic tension force of the dip-shaped magnetic loops, either in a normal-polarity configuration (Kippenhahn & Schlüter 1957) or in an inverse-polarity configuration (Kuperus & Raadu 1974). Whereas the corresponding global magnetic configuration in the latter case is typically a flux rope, as derived from coronal magnetic field extrapolations (e.g., Su & van Ballegooijen 2012), the magnetic configuration in the former case might just be a sheared arcade

* Supported by the National Natural Science Foundation of China.

system (Chen 2012), although theoretical models of flux ropes with the normal polarity configuration have also been proposed (e.g., Zhang & Low 2005).

Despite having been studied for decades, the formation of filaments is still a hot research topic in solar physics and has been discussed in a variety of works since filaments and the host magnetic structure are thought to be the progenitors of coronal mass ejections (Chen 2011). High-resolution observations have shown that the filament spine is composed of a collection of separate threads (Engvold 2004; Lin et al. 2005). These threads are believed to be the building blocks of filaments. So, to understand the formation of a filament, the formation of a filament thread should be explained in the first place. A filament thread is generally thought to be located along a flux tube. The magnetic field of quiescent or intermediate filaments is generally weak, e.g., several Gauss, while that of active region filaments is much stronger, e.g., tens of Gauss (Aulanier & Démoulin 2003). Therefore, for active region filaments, the formation of their threads can be simplified into a one-dimensional (1D) radiative hydrodynamic problem. Even for intermediate filaments, the 1D numerical simulation made by Zhang et al. (2012b) can still reproduce the oscillation behaviors revealed by satellite observations. Therefore, a 1D hydrodynamic model is still a good approximation even for intermediate filaments. More importantly, the relatively simple 1D radiative hydrodynamic simulations can provide a straightforward insight into the physics related to the formation and oscillation processes in solar filaments. For example, with 1D radiative hydrodynamic simulations, Antiochos et al. (1999) proposed the chromospheric evaporation plus coronal condensation model, where extra heating localized in the chromosphere drives chromospheric evaporation into the corona, and the dense hot plasma near the magnetic dip cools down to form a filament thread due to thermal instability.

In the chromospheric evaporation plus coronal condensation model, it was found that with the intermediately asymmetric heating at the two footpoints of a flux tube, a filament thread repeatedly forms and then drains down to the chromosphere. If the chromospheric heating at the two footpoints is relatively symmetric or the magnetic dip is deep enough, the filament thread would be held near the magnetic dip, continually growing (Karpen et al. 2001). Recently, Xia et al. (2011) performed state-of-the-art radiative hydrodynamic simulations of the filament thread formation process. It was found that once the coronal condensation happens, no further chromospheric heating is needed for the filament thread to grow. The siphon flow induced by the pressure imbalance between the chromosphere and the condensation would supply more and more plasma into the coronal condensation, leading to the continual growth of the filament thread. As the plasma accumulates, the gas pressure within the filament would increase, which hinders the siphon flow from the chromosphere. If so, an interesting question is raised, that is, for a given magnetic flux tube, what is the maximum length that a filament thread can grow. In this paper, we aim to investigate how long the filament thread would finally be and how the maximum length is related to the geometry of the magnetic flux tube. Our numerical method is introduced in Section 2, and the results are presented in Section 3, which are discussed in Section 4.

2 NUMERICAL METHOD

Similar to what we have done before (Xia et al. 2011; Zhang et al. 2012b,a, 2013), we deal with 1D radiative hydrodynamic equations, where the magnetic field is not explicitly taken into account under the assumption that the plasma dynamics do not affect the magnetic field. Note that the shape of the magnetic flux tube is represented by the distribution of the field-aligned component of the gravity, $g_{\parallel}$. The hydrodynamic equations shown below are numerically solved by the state-of-the-art MPI-Adaptive Mesh Refinement-Versatile Advection Code (MPI-AMRVAC, Keppens et al. 2003, 2012):

$$\frac{\partial \rho}{\partial t} + \frac{\partial}{\partial s}(\rho v) = 0, \tag{1}$$

$$\frac{\partial}{\partial t}(\rho v) + \frac{\partial}{\partial s}(\rho v^2 + p) = \rho g_{\parallel}(s), \tag{2}$$

$$\frac{\partial E}{\partial t}+\frac{\partial}{\partial s}(Ev+pv)=\rho g_{\parallel}v-n_{\rm e}n_{\rm H}\Lambda(T)+\frac{\partial}{\partial s}\left(\kappa\frac{\partial T}{\partial s}\right)+H(s), \tag{3}$$

where ρ is the mass density, s is the distance along the magnetic loop starting from the left footpoint, v is the velocity, p is the gas pressure, T is the temperature and $g_{\parallel}(s)$ is the field-aligned component of the gravity at a distance s along the magnetic loop, which is determined by the geometry of the magnetic loop. In addition, $E=\rho v^2/2+p/(\gamma-1)$ is the total energy density, where $\gamma=5/3$ is the adiabatic index. The second term on the right-hand side of Equation (3) is the optically thin radiative cooling, where $n_{\rm e}$ is the number density of electrons, $n_{\rm H}$ the number density of hydrogen, and $\Lambda(T)$ the radiative loss coefficient. The third term on the right-hand side of Equation (3) is the heat conduction, where $\kappa=10^{-6}T^{5/2}\,{\rm erg\ cm^{-1}\ s^{-1}\ K^{-1}}$ is the Spitzer-type heat conductivity. The last term on the right-hand side of Equation (3), $H(s)$, is the volumetric heating rate. It includes the steady background heating H_0 and the localized chromospheric heating, whose expressions will be discussed at the end of this section. We assume a fully ionized plasma model and take $\rho=1.4\,m_{\rm p}n_{\rm H}$ and $p=2.3\,n_{\rm H}k_{\rm B}T$ considering the helium abundance ($n_{\rm He}/n_{\rm H}=0.1$), where $m_{\rm p}$ is the proton mass and $k_{\rm B}$ is the Boltzmann constant. To calculate the radiative energy loss coefficient $\Lambda(T)$, a second-order polynomial interpolation is taken to compile a high resolution table based on the radiative loss calculations using an accurate atomic collisional rate and a recommended set of quiet-region element abundances over a wide temperature range (Colgan et al. 2008).

As mentioned before, it is widely believed that a filament is hosted at the dip of a magnetic loop, and supported by its magnetic tension force. So, we adopt a symmetric loop including a magnetic dip, as shown in Figure 1. The loop, whose total length is L, is composed of two vertical legs with a length of s_1 for each, two quarter-circular shoulders with a radius r, and a quasi-sinusoidal-shaped dip with a half-length of w. The dip has a depth of D below the apex of the loop. Then, we define s_2 as $s_2=s_1+\pi r/2$, the altitude of the dip (h) as $h=s_1+r-D$, and the total length of the dip $2w$ as $2w=L-2s_2$. The corresponding $g_{\parallel}$ in Equations (2)–(3) is then expressed as follows:

$$g_{\parallel}=\begin{cases}-g_{\odot} & s\le s_1\,,\\ -g_{\odot}\cos\left(\frac{\pi}{2}\frac{s-s_1}{s_2-s_1}\right) & s_1<s\le s_2\,,\\ g_{\odot}\frac{\pi D}{2(L/2-s_2)}\sin\left(\pi\frac{s-s_2}{L/2-s_2}\right) & s_2<s\le L/2\,,\end{cases} \tag{4}$$

where $g_{\odot}=2.7\times10^2\,{\rm m\,s^{-2}}$ is the gravitational acceleration at the solar surface.

Our simulations start from a thermal and force-balanced equilibrium state. Initially, the background heating H_0 is included in order to balance the thermal conduction and radiative cooling. The plasma in the loop is static. Then, each simulation is divided into two steps: (1) Filament formation: Localized chromospheric heating H_1 is introduced symmetrically near the footpoints of the magnetic loop so that the chromospheric material is evaporated into the corona and later condenses at a certain stage due to thermal instability, and then a filament thread forms and grows at the center of the magnetic loop; (2) Relaxation: The localized heating H_1 is linearly ramped down to zero after

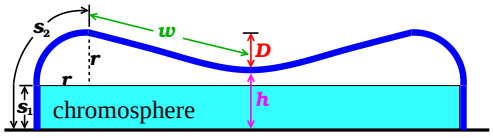

Fig. 1 Geometry of the magnetic loop used for the 1D radiative hydrodynamic simulations of the filament formation, where the thick line is the magnetic loop which is anchored to the solar chromosphere. Note that the horizontal and the vertical sizes are not to scale.

a decay timescale of 1000 s, and the chromospheric evaporation ceases. Owing to the disappearance of the evaporation flow, the compressed filament thread relaxes and expands. After that, the filament thread slowly grows in length due to the self-induced siphon flow as found by Xia et al. (2011). The formation and relaxation time will be described in Section 3.1.

In step 1, the volumetric heating rate $H(s)$ in Equation (3) is composed of two parts: the steady background heating $H_0(s)$ and the localized chromospheric heating $H_1(s)$. Their expressions are:

$$H_0(s) = \begin{cases} E_0 \exp(-s/H_m) & s < L/2\,, \\ E_0 \exp[-(L-s)/H_m] & L/2 \le s < L\,, \end{cases} \tag{5}$$

$$H_1(s) = \begin{cases} E_1 & s \le s_{\rm tr}\,, \\ E_1 \exp[-(s-s_{\rm tr})/\lambda] & s_{\rm tr} < s \le L/2\,, \\ E_1 \exp[-(L-s_{\rm tr}-s)/\lambda] & L/2 < s \le L - s_{\rm tr}\,, \\ E_1 & s > L - s_{\rm tr}\,. \end{cases} \tag{6}$$

The background heating term $H_0(s)$ is adopted to maintain the 1 MK corona with the amplitude $E_0 = 3 \times 10^{-4}\,{\rm erg\,cm^{-3}\,s^{-1}}$, and the scale height H_m is defined as $H_m = L/2$. The localized heating term H_1 is adopted to generate chromospheric evaporation into the corona with the amplitude $E_1 = 3 \times 10^{-2}\,{\rm erg\,cm^{-3}\,s^{-1}}$. The height of the transition region, $s_{\rm tr}$, is set to be $6\,{\rm Mm}$, and the scale height λ is $10\,{\rm Mm}$.

3 NUMERICAL RESULTS

3.1 Natural Growth via Siphon Flows

According to Xia et al. (2011), once coronal condensation happens, the filament thread can grow via siphon flows even without further localized chromospheric heating. In order to check how long the filament thread can grow, we perform a simulation of filament formation with parameters similar to those used in Xia et al. (2011), i.e., $s_1 = 5\,{\rm Mm}$, $r = 5\,{\rm Mm}$, $2w = 74.3\,{\rm Mm}$, $D = 1\,{\rm Mm}$ and $L = 100\,{\rm Mm}$. The evolution of the density distribution along the magnetic loop in step 1 is shown in the left panel of Figure 2. It is found that as localized heating H_1 is introduced near the two footpoints, the coronal part of the loop becomes hotter and denser. After 2 h, thermal instability occurs, and a segment of filament thread is formed as indicated by the high density near the loop center. As the chromospheric evaporation goes on, the filament grows with a rate of 0.2 km s^{-1}. Such a simulation in step 1 continues until the filament thread grows for 1 h. The length of the filament thread is $\sim$3 Mm. Then in step 2, we ramp down the localized chromospheric heating H_1 to zero in 1000 s. The corresponding evolution of the density distribution along the magnetic loop in step 2 is depicted in the right panel of Figure 2. It is seen that after the localized heating is switched off, the filament thread suddenly expands and then shrinks. Such an oscillation decays rapidly, and the filament thread soon reaches a quasi-equilibrium state, with a length of about 16 Mm. After that, the length of the filament thread slowly increases.

Figure 3 shows the growth of the length of the filament thread with time in step 2. It is found that as the localized heating and the resulting evaporation are switched off, the length of the filament thread first rapidly increases to 24 Mm, and then oscillates around 17 Mm. The oscillation decays rapidly, and then the length of the thread begins to slowly increase. It is seen that the growth rate decreases with time with an initial rate of 70 km h^{-1}. After about 120 h, the filament thread is 22.8 Mm long, and its growth rate becomes about 0.7 Mm per day, which means that the filament thread expands $\sim 1''$ per day. Such a rate is nearly imperceptible in observations that rely on visual inspection. So, we can consider that the length of the filament thread saturates at 22.8 Mm.

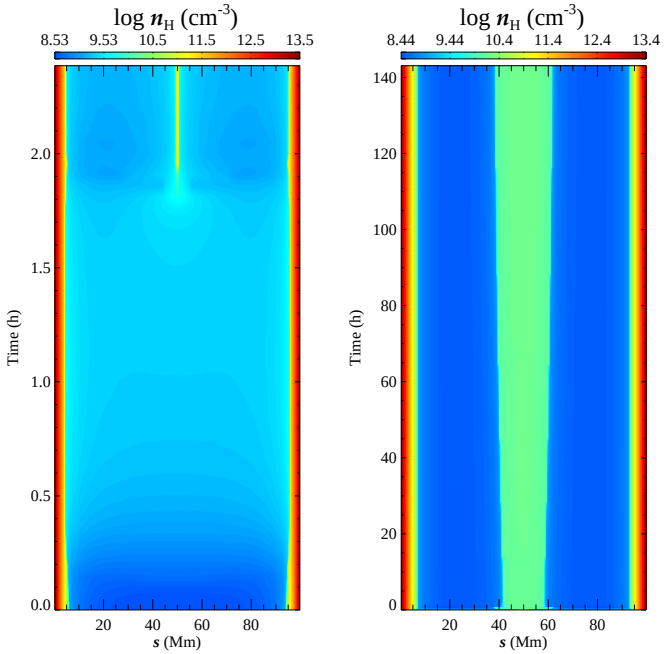

Fig. 2 Time evolution of the density distribution along the magnetic loop during the two stages: (a) the filament formation stage; (b) the self-growth stage.

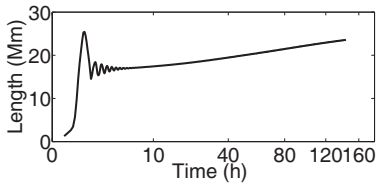

Fig. 3 Time evolution of the length of the filament thread in the relaxation stage.

3.2 Parameter Survey

We apply the method mentioned in Section 3.1 to investigate how the maximum length of the filament thread ($L_{\rm th}$) changes with the geometric parameters of the magnetic flux tube, i.e., the depth (D), the half-width (w) and the altitude (h) of the magnetic dip.

By fixing $w = 37.2$ Mm and $h = 9$ Mm, eight cases with D ranging from 0.4 Mm to 2.0 Mm are simulated. The variation in the length of the filament thread ($L_{\rm th}$) along with the depth of the magnetic dip (D) is shown in Figure 4. It is revealed that $L_{\rm th}$ decreases nearly linearly with increasing D. The scatterplot in Figure 4 can be fit with a linear function $L_{\rm th} = 23.6 - 0.91D$ (Mm). It can be noted that as D increases from 0.4 Mm to 2 Mm, the length of the filament thread only decreases $\sim$10%.

By fixing $D = 1$ Mm and $h = 9$ Mm, five cases with w ranging from 27.1 Mm to 42.1 Mm are simulated. The variation in the length of the filament thread ($L_{\rm th}$) along with the width of the magnetic dip (D) is shown in Figure 5. It is revealed that $L_{\rm th}$ increases linearly with increasing w, i.e., the length of the filament thread is longer for a wider magnetic dip. Their relation can be fit

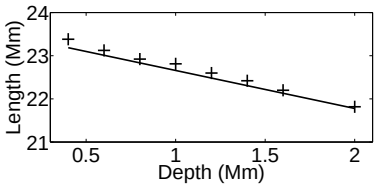

Fig. 4 Dependence of the length of the filament thread on the depth of the magnetic dip. The plus signs are from the numerical simulations, while the straight line represents the function which is fit for the whole parameter survey.

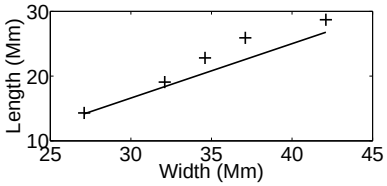

Fig. 5 The same as Fig. 4, but on the width of the magnetic dip.

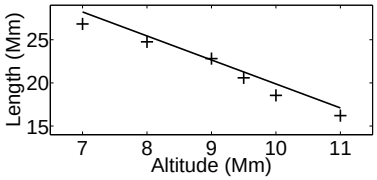

Fig. 6 The same as Fig. 4, but on the altitude of the magnetic dip.

with a function, $L_{\rm th} = 0.82w - 9.20$ (Mm). Such a straight line intersects the x-axis at $w = 11.2$ Mm, implying that under the conditions with $D = 1$ Mm and $h = 9$ Mm there exists such a threshold of the width of the magnetic dip, $w = 11.2$ Mm, below which no filament can be formed. This is qualitatively consistent with the criterion of thermal instability (Parker 1953).

By fixing $D = 1$ Mm and $w = 37.2$ Mm, five cases with h ranging from 7 Mm to 12 Mm are simulated. The variation in the length of the filament thread ($L_{\rm th}$) along with the altitude of the magnetic dip (h) is shown in Figure 6. It is revealed that $L_{\rm th}$ decreases with increasing h, i.e., the length of the filament thread is shorter for a higher magnetic dip. Their relation can be fit with a function, $L_{\rm th} = 43.56 - 2.48h$ (Mm). Such a straight line intersects the x-axis at $h = 17.6$ Mm, implying that under the conditions with $D = 1$ Mm and $w = 37.2$ Mm there exists such an upper limit for the altitude of the magnetic dip, $h = 17.6$ Mm, above which no filament can be formed.

4 DISCUSSION

More and more observational evidence tends to support the evaporation-condensation model for filament formation (e.g., Liu et al. 2012; Berger et al. 2008). Correspondingly, several groups have performed radiative hydrodynamic simulations, mainly in 1D, to confirm the model (e.g., Antiochos et al. 1999; Karpen et al. 2001; Luna & Karpen 2012; Xia et al. 2012). Recently, Xia et al. (2012)

extended the simulations from 1D to 2D. All their results revealed that as localized heating is introduced in the chromosphere, the local plasma is evaporated into the corona, and a cool filament is formed when the criterion of thermal instability is satisfied. The filament thread grows as the evaporation continues. Even when the chromospheric evaporation is switched off, the filament thread can still grow via siphon flows (Xia et al. 2011). However, as the siphon flows accumulate in the filament, its gas pressure will increase, which in turn hinders the siphon flows. Therefore, a crucial question is when the filament thread will stop growing. To answer this question, for the first time we performed 1D hydrodynamic simulations, which proceed until the length of the filament thread saturates in a prescribed flux tube with a magnetic dip. The parameter survey indicates that the maximum length ($L_{\rm th}$) of a filament thread is strongly related to the half-width (w), the depth (D) and the altitude (h) of the magnetic dip. Based on the numerical results, we derived a function for the dependence on each parameter. Since all the functions are linear, we describe the dependence of the length of filament threads with a multi-variable linear function, i.e., $L_{\rm th} = \alpha_1 w + \alpha_2 D + \alpha_3 h + \alpha_4$. The least squares fit to all the data points in Figures 4–6 yields

$$L_{\rm th} = (0.84 \pm 0.07)w - (0.88 \pm 0.27)D - (2.78 \pm 0.17)h + (17.31 \pm 3.07)\,,$$

where all the terms are in units of Mm. Such a fitted linear function is plotted in Figures 4–6 as straight lines.

Observations indicate that a filament is composed of a collection of threads (Lin et al. 2005). In quiescent filaments, the threads are generally short, whereas in active region filaments, the threads are relatively long (Mackay et al. 2010). These observations can be qualitatively explained by the simulation results presented in this paper: Active regions are born to be non-potential, implying the field lines are initially strongly sheared. In addition, active regions often experience fast rotations (Yan et al. 2008), which would further drag the magnetic field lines to become elongated, and the dips become shallow, i.e., the magnetic dips of active region field lines correspond to a large width (w) and a small depth (D). According to our formula, the corresponding filament threads would be long. On the other hand, quiescent filaments are formed in decayed active regions (van Ballegooijen & Martens 1989). Therefore, the corresponding magnetic fields might have a shorter w and larger D. As a result, the filament threads in quiescent filaments are shorter than those in active region filaments. Observations also indicate that quiescent filaments are located higher in the corona, e.g., 10^4–10^5 km, whereas active region filaments are often below 10^4 km in altitude (Mackay et al. 2010). Our result of the dependence of the length of the filament thread on the altitude of the magnetic dip implies that the longer threads of active region filaments are partly due to the low altitude of the magnetic dip.

It is noted that the simulations in this paper are aimed at studying the length needed for a filament thread to grow in a dipped magnetic flux tube in 5 days. In real observations, the lifetime of some filaments might be less than 5 days before they erupt when a certain instability happens (Chen et al. 2008; Shen et al. 2011). Besides, there is continual mass drainage from the filament to the chromosphere (Xia et al. 2011; Liu et al. 2012), so a filament thread in observations may have not yet reached its upper limit. However, as discussed above, the dependence of length of the filament thread on the altitude and the width of the magnetic dip can still qualitatively account for the typical characteristics of both quiescent and active region filaments qualitatively. In order to compare the simulation results with Hα observations more quantitatively, we plan to (1) do the extrapolation of the coronal force-free field based on the photospheric magnetic field observations, then (2) perform a series of 1D hydrodynamic simulations along many field lines retrieved from the extrapolation, and then (3) compare the simulated thread assembly with the Hα observations made by our ONSET telescope (Fang et al. 2013) in the partial-disk mode. This will be another step forward beyond Aulanier et al. (1999) and Gunár et al. (2013). It will also be interesting to check whether our scaling law for the length of the filament thread is applicable to the feet (or barbs) of the filaments as more and more observations of barbs have been made (e.g., Li & Zhang 2013).

Acknowledgements The authors thank the referee for useful comments. The research is supported by the National Natural Science Foundation of China (Grant Nos. 11025314, 10878002, 10933003 and 11173062) and the National Basic Research Program of China (973 program, 2011CB811402).

References

Antiochos, S. K., MacNeice, P. J., Spicer, D. S., & Klimchuk, J. A. 1999, ApJ, 512, 985
Aulanier, G., & Démoulin, P. 2003, A&A, 402, 769
Aulanier, G., Démoulin, P., Mein, N., et al. 1999, A&A, 342, 867
Berger, T. E., Shine, R. A., Slater, G. L., et al. 2008, ApJ, 676, L89
Chen, P. F. 2011, Living Reviews in Solar Physics, 8, 1
Chen, P. F. 2012, in The 3rd Hinode Science Meeting, Astronomical Society of the Pacific Conference Series, 454, Hinode-3, eds. T. Sekii, T. Watanabe, & T. Sakurai, 265
Chen, P. F., Innes, D. E., & Solanki, S. K. 2008, A&A, 484, 487
Colgan, J., Abdallah, J., Jr., Sherrill, M. E., et al. 2008, ApJ, 689, 585
Engvold, O. 2004, in IAU Symposium, 223, Multi-Wavelength Investigations of Solar Activity, eds. A. V. Stepanov, E. E. Benevolenskaya, & A. G. Kosovichev, 187
Fang, C., Chen, P.-F., Li, Z., et al. 2013, RAA (Research in Astronomy and Astrophysics), 13, 1509
Gunár, S., Mackay, D. H., Anzer, U., & Heinzel, P. 2013, A&A, 551, A3
Karpen, J. T., Antiochos, S. K., Hohensee, M., Klimchuk, J. A., & MacNeice, P. J. 2001, ApJ, 553, L85
Keppens, R., Nool, M., Tóth, G., & Goedbloed, J. P. 2003, Computer Physics Communications, 153, 317
Keppens, R., Meliani, Z., van Marle, A. J., et al. 2012, Journal of Computational Physics, 231, 718
Kippenhahn, R., & Schlüter, A. 1957, ZAp, 43, 36
Kuperus, M., & Raadu, M. A. 1974, A&A, 31, 189
Li, L., & Zhang, J. 2013, Sol. Phys., 282, 147
Lin, Y., Engvold, O., Rouppe van der Voort, L., Wiik, J. E., & Berger, T. E. 2005, Sol. Phys., 226, 239
Liu, W., Berger, T. E., & Low, B. C. 2012, ApJ, 745, L21
Luna, M., & Karpen, J. 2012, ApJ, 750, L1
Mackay, D. H., Karpen, J. T., Ballester, J. L., Schmieder, B., & Aulanier, G. 2010, Space Sci. Rev., 151, 333
Martin, S. F. 1998, Sol. Phys., 182, 107
Ning, Z., Cao, W., & Goode, P. R. 2009, ApJ, 707, 1124
Parker, E. N. 1953, ApJ, 117, 431
Shen, Y.-D., Liu, Y., & Liu, R. 2011, RAA (Research in Astronomy and Astrophysics), 11, 594
Su, Y., & van Ballegooijen, A. 2012, ApJ, 757, 168
Tandberg-Hanssen, E., ed. 1995, The Nature of Solar Prominences, Astrophysics and Space Science Library, 199
van Ballegooijen, A. A., & Martens, P. C. H. 1989, ApJ, 343, 971
Xia, C., Chen, P. F., Keppens, R., & van Marle, A. J. 2011, ApJ, 737, 27
Xia, C., Chen, P. F., & Keppens, R. 2012, ApJ, 748, L26
Yan, X. L., Qu, Z. Q., & Xu, C. L. 2008, ApJ, 682, L65
Zhang, M., & Low, B. C. 2005, ARA&A, 43, 103
Zhang, P., Fang, C., & Zhang, Q. 2012a, Science in China G: Physics and Astronomy, 55, 907
Zhang, Q. M., Chen, P. F., Xia, C., & Keppens, R. 2012b, A&A, 542, A52
Zhang, Q. M., Chen, P. F., Xia, C., Keppens, R., & Ji, H. S. 2013, A&A, 554, A124
Zirker, J. B. 1989, Sol. Phys., 119, 341